Hyperspectral Imaging to Quantify Nodules and Detect Biological Nitrogen Fixation in Legumes

Authors: Yuchen Wang[1*†], Kithmee De Silva[1*†], Di Song[2*], Mohammed Kamruzzaman[2]

Affiliations:

[1]Department of Plant Biology, University of Illinois at Urbana-Champaign;

[2]College of ACES, Department of Agricultural & Biological Engineering, University of Illinois, Urbana-Champaign

[*]These authors contributed equally to this work.

[†]Corresponding author. Email: yuchen26@illinois.edu, kithmee2@illinois.edu

Abstract

Legume root nodules are important for biological nitrogen fixation, a process critical for plants to gain additional nitrogen from the environment. Nodule quantification is valuable for evaluating nitrogen fixation efficiency, assessing symbiotic relationships, monitoring responses to nitrogen, and supporting genetic studies on legume adaptation and productivity. However, accurate quantification of root nodules is difficult and time-consuming due to the complexity of the root system and soil interference. Here, we explore the utility of hyperspectral imaging as a non-destructive tool to detect active fixing root nodules with minimal preparation and show that we can differentiate nodules and root tissues through unique spectral signatures while also distinguishing between fixing and non-fixing nodules. We applied deep learning techniques to develop an automated nodule counting pipeline adaptable across different legume species and under diverse growth conditions. This approach eliminates the need for labor-intensive counting and enables the detection of nodules embedded within dense root tangles with high accuracy. This automated hyperspectral approach offers a promising alternative to support assessments of nodule abundance and their activity across legume species grown under various environments.

Key Words: Hyperspectral Imaging, Plant Symbiosis, Nodule Quantification, Machine Learning

Introduction

Legumes (Fabaceae or Leguminosae family), the third largest family of angiosperms, are known for their worldwide distribution and agricultural value. Their ability to form a symbiotic relationship in root nodules with nitrogen-fixing rhizobia in the soil distinguishes them from non-nodulating plants. This association enables the conversion of atmospheric nitrogen (N_2) into ammonia (NH_3), a biologically usable form of nitrogen that supports plant growth. In return, the plant supplies the bacteria with carbon derived from photosynthesis. This process, known as biological nitrogen fixation (BNF), reduces reliance on synthetic nitrogen fertilizers and allows legumes to thrive in nitrogen-poor soils, contributing to sustainable agriculture (Peoples et al., 1995). Studies suggest that BNF may give legumes a competitive advantage over non-fixing plants under future elevated CO_2 levels as the additional nitrogen gained helps maintain the plants' carbon-to-nitrogen balance (Rogers et al., 2009).

This symbiosis is facilitated by specialized root structures called nodules, which house the bacteria and create a microenvironment suitable for the oxygen-sensitive enzyme nitrogenase. Leghaemoglobin, a heme protein found in nodules, binds free oxygen to maintain the low-oxygen conditions required for nitrogenase function while transporting O^2 to bacteria for respiration (Appleby, 1984; Ott et al., 2005). However, nodulation and nitrogen fixation are known to vary, both within and among legume species (Bourion et al., 2007; Hardarson et al., 1993; Iqbal et al., 2022). This variability results from a complex interplay of genetic and environmental factors, as the host primarily shapes nodule morphology and structure while the efficiency of nitrogen fixation is largely determined by the bacterial symbiont partners (Mortier et al., 2012; Sprent, 2007). Different legume species (and even different genotypes within a species) can exhibit distinct nodule characteristics, including variations in number, size, weight and morphology (Sprent et al.,

55 2017). For instance, some legumes develop determinate nodules with a spherical, fixed size, while
56 others form cylindrical indeterminate nodules that continue to grow and display meristematic
57 activity. These inherent differences not only affect the total capacity for nitrogen fixation but also
58 influence the efficiency and longevity of the symbiosis (Bourion et al., 2007; Tajima et al., 2007).
59 Nodule phenotypic traits such as number, size, biomass, internal hue/pigmentation, and
60 external morphology have been frequently used as proxies for BNF capacity (Hensley et al., 2021;
61 Tajima et al., 2007). Traditional methods, such as manual counting and nodule area estimation
62 (Dias et al., 2017; Tajima et al., 2007) have been complemented by advances in imaging that enable
63 semi-automated nodule quantification through both destructive and non-destructive approaches.
64 Destructive methods include direct quantification of isolated nodules (Barbedo, 2012; Dias et al.,
65 2017; Vikman and Vessey, 1993) and microscopic assessment on nodule cross sections (Tajima et
66 al., 2007; TSYGANOV et al., 2002), while non-destructive approaches involve imaging minimally
67 disturbed field-grown roots using minirhizotron platforms (Rowland et al., 2015), digital scans of
68 washed intact root systems (Lira and Smith, 2000), and rhizoboxes (Nagel et al., 2012). Despite
69 these improvements in throughput, they remain time-consuming, labor-intensive, and are
70 confounded by the high variability in nodule size, shape and texture, and the inherent clustered
71 nature of nodules. Also, these morphological indicators often correlate poorly with actual nitrogen
72 fixation, in part because nodules at different developmental stages, including senescent ones, can
73 appear similar yet differ drastically in metabolic activity (Dupont et al., 2012; Fernández-Luqueño
74 et al., 2008; Vikman and Vessey, 1993). To address this, biochemical assays such as
75 leghaemoglobin extraction (Wilson and Reisenauer, 1963) and acetylene reduction (Hardy et al.,
76 1968; Vance et al., 1979) assess nodule function more directly. However, these assays are
77 destructive, involve hazardous chemicals, and lack precision across diverse nodule types and

developmental stages. Collectively, these constraints highlight the need for non-destructive, functionally informative, and scalable approaches to quantify BNF accurately.

Unlike conventional RGB imaging, which relies on morphological cues, hyperspectral imaging (HSI) captures reflectance spectra across hundreds of narrow, contiguous wavelengths, enabling the detection of subtle biochemical and structural differences. This spectral sensitivity is particularly relevant given that internal pigmentation gradients in nodules, linked to nitrogen-fixing activity, may produce detectable signatures in hyperspectral data (Chung et al., 2020; Hensley et al., 2021). HSI has been effectively used to monitor plant physiological processes such as stress responses (Behmann et al., 2014) and disease progression (Berdugo et al., 2014), indicating its potential for assessing nodule function.

Complementary advances in deep learning, especially convolutional neural networks (CNNs), have enabled accurate nodule segmentation from high-resolution RGB images of soybean roots (Woo et al., 2023). Utilizing CNNs, the YOLO (You Only Look Once) series, a deep learning object detection algorithm, stands out for its speed and accuracy. Since its introduction as a single-stage detection algorithm, YOLO has rapidly evolved to include multi-scale feature extraction, attention mechanisms, and transformer-based modules (Redmon et al., 2015). YOLOv11 builds upon these advancements to achieve high precision with reduced computational load, making it well-suited for root nodule detection in complex soil environments. Therefore, integrating spectral information with deep learning-based models can improve both the precision and the physiological relevance of an automated nodule detection model.

In this study, we present an HSI-based pipeline integrated with deep learning to non-destructively identify and quantify root nodules. By leveraging the spectral sensitivity of HSI and the strong object detection capabilities of the deep learning algorithm YOLOv11, we developed a

model capable of distinguishing actively nitrogen-fixing nodules under varied soil conditions. Then, we applied our detection pipeline to five legume species to demonstrate its broad applicability across a range of morphologies and nodule types. Finally, we evaluate model performance, explore spectral features associated with functional nodules, and demonstrate the scalability of this approach for high-throughput root phenotyping in a real research experiment.

Materials and Methods

Plant materials and growth conditions

Five legume species, common bean (*Phaseolus vulgaris)*, soybean (*Glycine max*), cowpea (*Vigna unguiculata*), *Medicago truncatula,* and red clover (*Trifolium repens*) were used in this study. Scarified and imbibed medicago seeds were vernalized for 48 h in the dark at 4 °C, incubated for 24 h at room temperature and germinated on 1% agar plates vertically in a growth chamber under 200 μmol m^{-2} s^{-1} for 72 h. The seedlings were transferred to 4" pots containing either sterile potting medium (BM6 All-Purpose, Berger, Québec, Canada) or 1:1 mixture of coarse calcined clay (Turface MVP, PROFILE, Buffalo Grove, IL, USA) and fine clay (Greens Grade, PROFILE, Buffalo Grove, IL, USA). Common bean seeds were surface sterilized and germinated on dampened filter paper placed on a petri dish for 48 h. The seeds with radicles were transplanted in 6" pots with 1:1 mixture of coarse calcined clay (Turface MVP, PROFILE, Buffalo Grove, IL, US) and fine silica sand. Soybean, cowpea and clover seeds were directly sown in 6" pots with mixture of coarse calcined clay and fine silica sand. *Medicago* and clover plants were grown under a light intensity of 300 μmol m^{-2} s^{-1} under 8/16 h day/night cycle, 24/22 °C day/night temperature regime and 65% humidity while common bean, soybean and cowpea were grown under 800 μmol m^{-2} s^{-1} under 12/12 h day/night cycle, 28/25 °C day/night temperature regime and 65% humidity.

The plants were inoculated with rhizobacteria either sowing into the soil or by directly applying to the base of the plantlet 3 days after transplanting (details of rhizobial strains in Table S1). The plants were supplemented with 0.1x fertilizer (Schultz All Purpose Plant Food 20-20-20, Knox Fertilizer, Knox, IN, USA) once a week to promote nodule formation under nitrogen-limiting conditions. All plants were watered every two days to maintain uniform soil moisture.

Rhizobox design

The rhizobox was assembled using a darkened acrylic back panel and a transparent front panel made of glass, secured within a wooden frame with drainage holes at the base. The rhizobox has dimensions of 27 cm × 23 cm × 4 cm (height × width × depth). Soybean seedlings germinated in soil for five days were transplanted into rhizoboxes filled with either potting medium (BM6 All-Purpose, Berger, Québec, Canada) or fine silica sand. The rhizoboxes were positioned at a 45° angle with the glass panel facing downward to encourage root growth along the transparent surface. The glass surface was covered with aluminum foil to minimize light exposure to the roots.

Nodule sampling and hyperspectral image collection

Roots were harvested and thoroughly rinsed with distilled water to remove residual soil particles, taking care not to damage the nodules. The harvested root can be stored in -80 ºC if images are not planned to be taken within 24 hrs. Before imaging, excess water was gently removed while ensuring the roots remained moist to prevent desiccation. The roots were then carefully spread out to ensure even distribution and uniform height, minimizing nodule overlap and facilitating accurate identification. For samples grown in rhizoboxes, imaging was conducted directly through the glass panel. Hyperspectral data were collected from each root sample for subsequent analysis. Following imaging, nodules were manually counted with direct observation

146 from the root to compare with model performance. A subset of roots was stored at -80 °C for
147 biochemical assays.

148 *Nodule absorbance scan and leghaemoglobin quantification assay*

149 Frozen root samples from 6-week-old common beans grown under minimal nitrogen in a
150 1:1 mixture of coarse calcined clay and fine clay were carefully separated into 'green' nodules,
151 'pink' nodules and root tissue. For each type, 1 g of tissue was weighed and crushed in liquid
152 nitrogen. Total protein was extracted using 1 mL of 1x phosphate buffered saline (PBS, Corning
153 21-040-CV). The samples were centrifuged at 10,000 g for 15 minutes to pellet the debris. The
154 absorbance spectra of the clarified supernatant were measured from 400 to 1000 nm with 2 nm
155 step increments using the TECAN Infinite 200 PRO series microplate reader.

156 The spectrophotometric leghaemoglobin assay was done as described by Senthilkumar et
157 al. (Senthilkumar et al., 2021). The supernatant from each sample was diluted fourfold (1:4) with
158 1x PBS buffer. An equal volume of alkaline pyridine reagent (4.2 M Pyridine in 0.2 M NaOH)
159 was added. This mixture was split into two aliquots, of which one was treated with a few crystals
160 of sodium dithionate, and the other with potassium hexacyanoferrate. Absorbance was measured
161 using the microplate reader at 556 nm and 539 nm for sodium dithionate-treated and potassium
162 hexacyanoferrate-treated samples, respectively. Leghaemoglobin content was calculated by the
163 following equation (where D is the dilution factor) and normalized for the initial tissue weight ;

164 $$\textit{Leghaemoglobin concentration (mM)} = ((A_{556} - A_{539}) \times 2D)/ 23.4$$

165 *Hyperspectral Camera Setup*

166 Hyperspectral images were acquired using a line-scan benchtop HSI system (Resonon Inc.,
167 Bozeman, MT, USA) operated in a controlled dark environment. The system consisted of a 900-
168 pixel line-scan hyperspectral camera (Pika L, Resonon Inc.) covering a spectral range of 374–1015

nm with a spectral resolution of 2.7 nm, yielding a total of 281 spectral bands. The imaging setup also included a linear translation stage for sample movement and a computer equipped with Spectronon Pro software (Resonon Inc.) for system control and data acquisition. The camera offered a maximum spatial resolution of 900 × 900 pixels and supported frame rates up to 249 fps. Prior to analysis, raw hyperspectral data were corrected for system noise and illumination variability by applying dark correction (removing sensor background signal) and white reference correction (normalizing reflectance using a calibrated white reference panel). These corrections were performed automatically using the software to ensure accurate reflectance spectra for all pixels across the image.

Hyperspectral Imaging process

After acquiring full-range hyperspectral data, reflectance values at 660 nm, 550 nm, and 470 nm were extracted to generate standard RGB composite images. In parallel, reflectance at 515 nm, 560 nm, and 600 nm—wavelengths identified as showing spectral differentiation between root and nodule tissues—were selected to construct 'enhanced images'. To enhance the contrast between nodules and root tissue, we computed a pixel-wise slope across these three hyperspectral bands. First, slope_1 was calculated between 515 nm and 560 nm. Next, slope_2 was calculated between 550 nm and 600 nm. The final pixel value for the enhanced image was obtained by subtracting slope_1 from slope_2. The resulting slope image was normalized to a grayscale range (0–255) to enhance nodule visibility and support segmentation.

Model training and generation of validation data

After generating RGB and enhanced images, each image was manually annotated using the web-based annotation tool MakeSenseAI (Skalski, 2019). The total number of nodules identified per image was recorded to serve as a reference for model evaluation. The annotated label

192 coordinates, along with the corresponding images, were used to train object detection models using
193 YOLOv11. To account for physiological differences in nodule development, the dataset was
194 divided into two categories: determinate and indeterminate nodules. Separate models were trained
195 for RGB images and enhanced hyperspectral images within each nodule category to evaluate
196 detection performance across both image types. A separate validation dataset that comprises RGB
197 and enhanced images not seen during training was used to assess model performance (details of
198 datasets in Table S2). For each validation image, the trained model outputs the total number of
199 detected nodules, along with predicted bounding box coordinates and associated probability
200 scores. A confidence threshold was applied to confirm valid nodule detections. To compare the
201 predicted counts with image counts and visual counts, Pearson correlation analyses were
202 performed using the cor() function in R (version 4.5.0). The relative accuracy of the predicted
203 counts was calculated using the following equation:

204 *Absolute Percentage Error (APE) = |(Predicted Counts - Image Counts)/Image Counts|*

205 *Experiment Setup and Physiological measurements*

206 Common bean and *Medicago truncatula* were grown in a factorial condition with varying
207 nitrogen treatments and CO_2 levels (details of the experiment setup in Table S3). After harvesting
208 the roots, both shoots and root tissues were dried at 65 °C for 96 h for biomass quantification (root
209 biomass include nodules). The nitrogen use efficiency (NUE) and nodule density were calculated
210 using the following equations:

211 *NUE = Dry total biomass (mg) / Nitrogen treatment (mM)*

212 *Nodule Density = Nodule number (Visual counts) / Dry root biomass (mg)*

213 A three-way ANOVA followed by Tukey's test was performed to assess the effects of nitrogen
214 level, CO_2 level, and count type (predicted vs. visual) on nodule counts. Pearson correlation

215 analyses were conducted using the cor() function in R (version 4.5.0) to evaluate the relationships
216 between physiological measurements and nodule counts.
217
218 **Results**
219 *Legumes exhibit species-specific nodule morphology*
220 Five legume species were selected for this study, representing a range of nodule
221 developmental types. These included three determinate species, common bean (*Phaseolus*
222 *vulgaris*), cowpea (*Vigna unguiculata)* and soybean (*Glycine max*); two indeterminate species,
223 *Medicago truncatula* and red clover (*Trifolium repens*). To capture a broader nodule physiological
224 variation, experimental conditions including growing media, growth duration and nutrient
225 supplementation regimes were varied while maintaining optimal growth conditions for each
226 species (Table S1).
227 We observed noticeable differences in nodule size, density and morphology across the five
228 legume species (Figure 1A), with a clear distinction between determinate and indeterminate nodule
229 types (Figure 1B). Indeterminate nodules, as seen in *Medicago* and clover, formed elongated,
230 branched nodules. Determinate nodules of common bean, cowpea and soybean were round and
231 often formed clusters. Size of nodules also varied greatly within each plant individual due to their
232 developmental stages. A consistent pattern across species was the external nodule coloration
233 associated with nitrogen-fixing activity (Navascués et al., 2012). Pink coloration, typically
234 associated with leghaemoglobin content, indicates active nitrogen fixation, while green or white
235 nodules often indicate inactive or senescing nodules as the heme content degrades (Dupont et al.,
236 2012). In all species except soybean, nodules typically showed pink and green hues externally. In

contrast, soybean nodules appeared uniformly brown on the surface, but upon dissection, internal tissue color ranged from pink to green, reflecting different functional states.

Hyperspectral signatures capture biochemical differences between nodules and root tissue

Although legumes exhibit species-specific nodule morphology, nodules across species share a fundamental protein composition required to facilitate symbiosis and nitrogen fixation, and this protein profile is distinct from that of root tissues (Mergaert et al., 2020; Ott et al., 2005). As an initial assessment of whether biochemical and compositional differences between nodules and root tissue influence spectral properties, we separately isolated each tissue type and extracted total protein content. Absorbance scans of the protein extracts revealed distinctly different spectral profiles between the two tissues (Figure 1C), supporting the hypothesis that hyperspectral imaging may capture these differences in situ.

For imaging, we selected plants of each legume species aged 4-6 weeks with well-developed nodules and thoroughly cleaned the root systems to remove all potting media. First, to identify informative hyperspectral wavelengths, we performed full-spectrum reflectance scans using the Resonon HSI system. Regions of interest were visually selected based on RGB images to compare spectral reflectance across tissue types. This revealed distinct differential peaks at 515, 560, and 600 nm (Figure 1D). These three spectral bands were subsequently processed to generate an enhanced image (hereafter referred to as the "enhanced image"). These enhanced images helped the visual distinction of nodules from root tissues, where clusters of dark pixels (black dots) correspond to areas of active nodule presence, while root tissue blends into the lighter gray background. An example of an RGB image alongside its corresponding enhanced image after processing is shown in Figure 1E.

Enhanced imaging selectively identifies functional/active nodules

An unexpected observation from enhanced images was the spectral difference between green and pink nodules on common beans, with green nodules appearing to be more similar to root tissue than nodules (Figure 1E). Given that green nodules are typically senesced (Navascués et al., 2012), the presence of active leghaemoglobin in pink nodules likely drives this spectral distinction, consistent with their characteristic coloration. In *Medicago* mutants such as *does not fix (dnf)*, which lack leghaemoglobin in their nodules (Starker et al., 2006) also showed no spectral differences compared to root tissue (Figure S1). Further quantification of leghaemoglobin content in nodules revealed significantly lower, almost undetectable levels of leghaemoglobin in green nodules (Figure 1F). The leghaemoglobin assay findings support that the spectral distinction is a result of this molecule, and also highlight a key feature of our approach, the selective identification of actively nitrogen-fixing nodules within the root system.

This approach effectively distinguished nodule tissue from surrounding root and background material with minimal cleaning of root systems for accurate imaging. Furthermore, the use of different growth media revealed that calcined clay emitted a reflectance similar to nodules (Figure 1G), making it challenging to work with unless thoroughly cleaned to prevent misidentification. However, general potting mix (BM6) and silica sand did not interfere with the nodule identification process (Figure 1G). Additionally, direct imaging of roots in rhizoboxes was feasible when using non-interfering substrates (Figure S2).

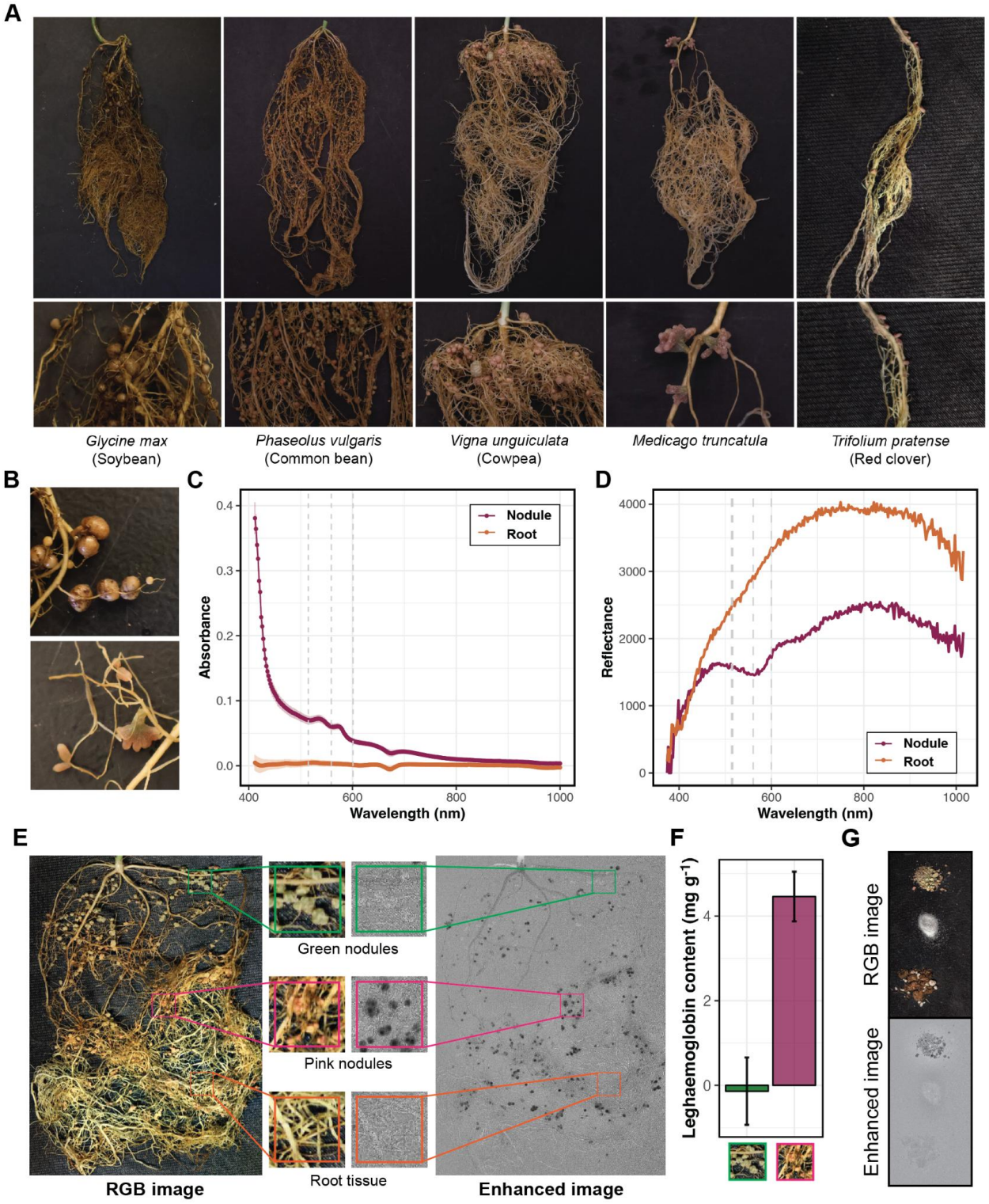

Figure 1 Hyperspectral imaging captures morphologically and physiologically diverse legume nodules through reflectance associated with leghaemoglobin. (A) Root systems and nodules of the

five legume species selected for this study. (B) Representative images of indeterminate (top) and determinate (bottom) nodule types. (C) Absorbance spectra of protein extracts from isolated nodules and root tissue. (D) Reflectance spectra of different root tissue types. (E) RGB and enhanced images of a common bean root system, illustrating how different tissue types are represented in each image. (F) Quantification of legheamoglobin content in green and pink nodules in common bean (n=3). (G) Hyperspectral signatures of various potting media; clay, sand and potting mix (BM6), shown from top to bottom.

Nodule-type specific training improves nodule detection

Given the clear separation of nodules in enhanced images, we deemed them to be well-suited for automated feature extraction, motivating us to apply deep learning–based models for nodule quantification. For this, following spectral enhancement to differentiate nodules from the background root tissue, images were preprocessed for object detection model development. Specifically, bands 450, 550, and 670 nm were combined to generate RGB images, while bands 515, 560, and 600 nm were used to create enhanced images optimized for nodule visualization (Figure 2A). Common bean root images in both enhanced and RGB format were manually annotated using MakeSenseAI (Skalski, 2019) to generate the training datasets for an object detection model using YOLOv11 (Jocher and Qiu, 2024) (Figure 2B). RGB and enhanced models were trained and evaluated in parallel using identical pipelines (Figure 2A). An independent validation set comprising images of common bean and *Medicago* roots was used to assess model performance.

This model, trained on common beans (determinate nodules), exhibited poor generalization when applied to *Medicago* (indeterminate nodules), frequently overcounting due to branched

305 indeterminate nodules being incorrectly identified as multiple individual nodules (Figure S3). To
306 resolve this, we trained separate object detection models for each nodule morphotype: a
307 determinate model using common bean root images, and an indeterminate model using *Medicago*
308 root images, both following the same training pipeline (see Table S2 for dataset details).
309 Performance of each model was evaluated by comparing predicted nodule counts (generated by
310 the model) to image counts (manually annotated on the same image) and visual counts (directly
311 observed from the root system by the naked eye). In both models, predicted counts were strongly
312 correlated with manually annotated image counts ($R^2 > 0.93$; Figure 2C), confirming that
313 morphotype-specific training substantially enhances detection accuracy.
314
315 *Enhanced hyperspectral model outperforms the RGB-based model in detecting nodules*
316 Predicted counts were compared to image counts to assess alignment with manual
317 annotations on the same image, and to visual counts to account for nodules potentially missed due
318 to imaging angle, root density, or other obstructions. For enhanced images, image counts included
319 only active nodules identified by spectral signatures, whereas visual counts included all visible
320 nodules regardless of activity.
321 Overall, nodule detection trends for both nodule types showed strong positive correlations
322 with both images and visual counts (coefficient of determination (R^2) > 0.82 and Pearson
323 correlation coefficient (r) > 0.74; Figure 2C). The predicted counts aligned more closely with
324 image counts than visual counts, particularly for indeterminate nodules. The discrepancy between
325 predicted and visual counts was more pronounced in the determinate model, where enhanced
326 images yielded r = 0.93 with image counts and r = 0.82 with visual counts. For both morphotypes,
327 models trained on enhanced images consistently outperformed those using RGB images, likely

328 due to reduced background noise. However, in both models, enhanced images consistently
329 detected more nodules than RGB images, evident in both the quantitative counts (Figure 2C) and
330 during visual inspection (Figure 2B). In the indeterminate model, predictions from both image
331 types aligned more closely with manual counts than in the determinate model, though RGB-based
332 predictions still underestimated nodule numbers (Figure 2C).

333 Detection accuracy from enhanced images was assessed using mean Absolute Percentage
334 Error (APE) against both image and visual counts (Figure 2D). Overall, error rates were lower for
335 determinate than indeterminate nodule images, and increased when compared to visual counts.
336 Relative to image counts, APE for determinate nodules remained low (12–15%) across all count
337 bins. However, when assessed against visual counts, APE exceeded 50% at low nodule numbers,
338 decreasing with higher counts (Figure 2D). The mean APE relative to image counts was higher for
339 the indeterminate model, ranging from 25% to 60%, and increased with nodule abundance (Figure
340 2D). As with determinate nodules, APE values were further elevated when predictions were
341 benchmarked against visual counts (Figure 2D).

342

343 *Morphotype-specific models enable cross-species nodule detection*

344 To evaluate cross-species applicability, the determinate and indeterminate nodule detection
345 models trained on common bean and *Medicago*, respectively, were applied to soybean, cowpea,
346 and red clover. The determinate model, used for cowpea and soybean, performed well on cowpea,
347 with predicted counts closely tracking image-based counts ($R^2 = 0.87$), though overestimation was
348 more pronounced in roots with higher nodule counts (Figure 2E). In contrast, performance on
349 soybean was weaker ($R^2 = 0.73$), with consistent overprediction across all count levels, suggesting
350 morphological divergence between the species was not captured by the training data. The

indeterminate model applied to red clover showed a strong correlation with image-based counts ($R^2 = 0.94$). The model produced more accurate predictions on images with fewer nodules, while a slight overestimation was observed in images with higher nodule counts (Figure 2E). Both models performed optimally on the species used for training. Although model performance varies by species, the two trained models provide a scalable framework for nodule detection across legumes with similar nodule morphotypes.

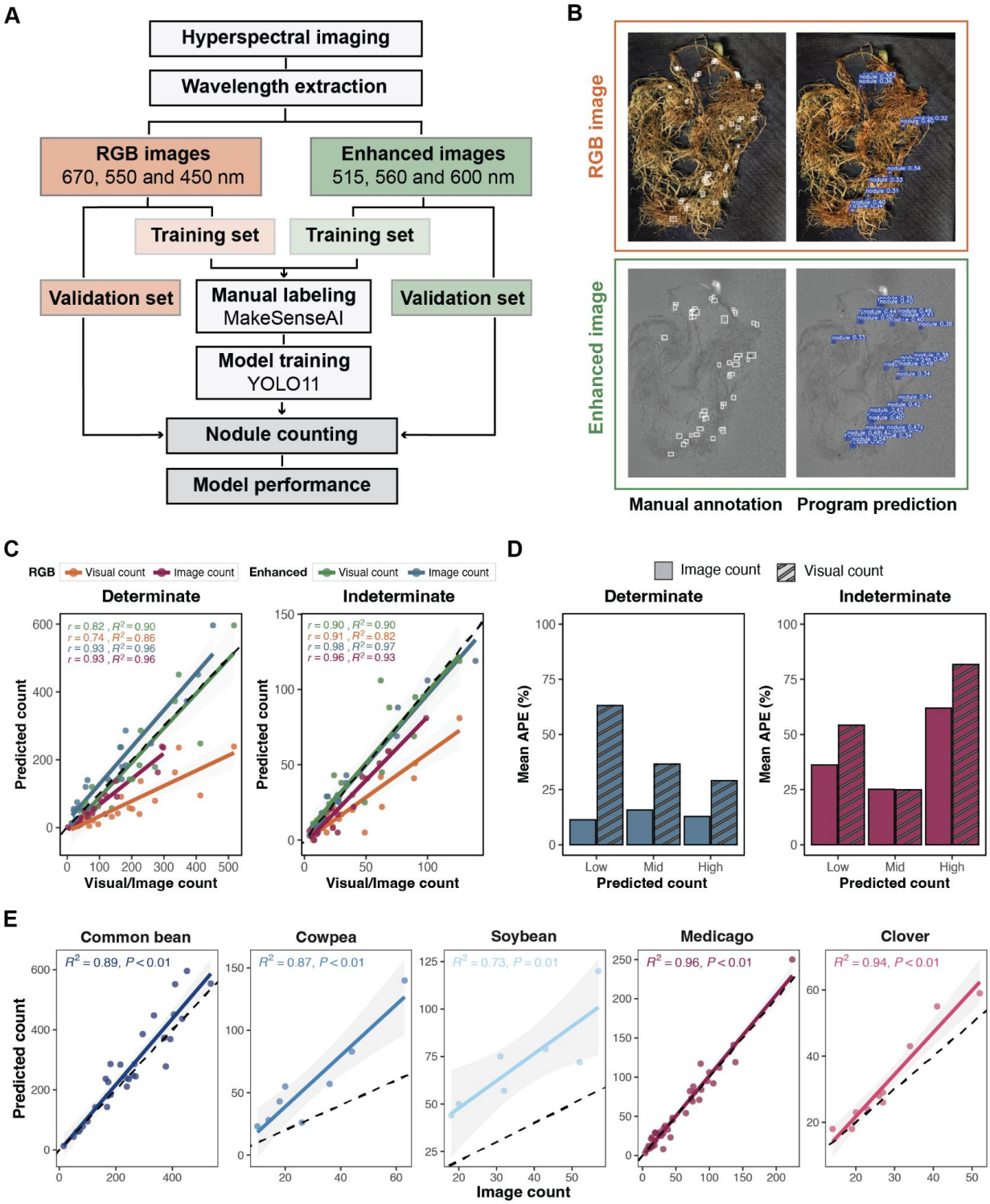

Figure 2 Training a machine learning model to accurately detect nodules using enhanced hyperspectral images and RGB images. (A) Flowchart outlining the steps used in model training and validation. (B) Representative images of manually annotated nodules and model-predicted

nodules on enhanced and RGB images of common bean roots. (C) Correlation between model predictions and visual and image counts using enhanced and RGB images (color-coded as indicated in the legend). Pearson correlation coefficients (r) and coefficients of determination (R^2) for each group are shown within the plot. (D) Mean absolute percentage error (APE) in detecting determinate and indeterminate nodules using enhanced images. Results are grouped into low, mid and high bins based on predicted count distribution. (APE = abs(Visual/Image count - program count)/Visual/Image count*100). (E) Model performance across different legume species.

Case Study: Nodule detection model links symbiosis in response to environmental cues

To demonstrate the practical and biological relevance of the nodule detection model, we applied it in a controlled experiment simulating real-world environmental responses. Nodulation is closely linked to the plant's overall nitrogen status, and legumes adjust their symbiotic interactions in response to environmental conditions. Physiologically, it is well known that both soil nitrate levels and atmospheric CO_2 concentrations influence the symbiotic process: high nitrate levels inhibit nodulation (van Noorden et al., 2016), whereas elevated CO_2 promotes it (Libault, 2014; Rogers et al., 2009). Both factors play a role in optimizing the plant's resource allocation and nutrient use efficiency.

We grew common bean and *Medicago truncatula* under a factorial design incorporating combinations of low/high nitrogen conditions, and ambient/elevated CO_2 levels (Figure 3A, details in Table S3). Root systems were imaged using hyperspectral imaging, and nodule counts were obtained using our nodule detection model. In parallel, visual counts were recorded from the roots to serve as a reference to evaluate model performance. Overall, the nodule detection model produced predicted nodule counts comparable to visual nodule counts, effectively capturing the

385 dynamics of nodulation in response to varying nitrogen and carbon availability in the growth
386 environment (Figure 3B and C). Specifically, both the determinate and indeterminate detection
387 models successfully captured the upregulation of nodulation under elevated CO_2 conditions
388 (Figure 3B). The effect of nitrogen level on downregulation of nodulation was more pronounced
389 in the determinate model, whereas it was present but less apparent in the indeterminate model
390 (Figure 3C).

391 Since our detection model quantifies actively nitrogen-fixing nodules, we further examined
392 the relationship between nodule counts and physiological measurements to assess the contribution
393 of symbiotically assimilated nitrogen to overall plant growth. Pearson correlation analyses were
394 performed between both predicted and visual nodule counts and various physiological traits
395 (Figure 3D). First, we observed a strong correlation between predicted and visual nodule counts,
396 indicating successful detection by our model (Figure 3D). Furthermore, nodule counts showed
397 positive correlations with shoot biomass, root biomass, and NUE, suggesting that greater
398 nodulation is associated with enhanced plant growth and nutrient acquisition (Figure 3D). Nodule
399 counts showed a negative correlation with nitrogen treatment level, providing further evidence of
400 the inhibitory effect of nitrate on nodulation (Figure 3D).

401 Next, we assessed whether the nodule detection model could capture environmentally
402 driven patterns in nodulation linked to biomass. Under low nitrogen, predicted nodule counts were
403 more strongly correlated with shoot biomass, suggesting greater reliance on symbiosis when
404 nitrogen is limited (Figure 3E). In contrast, elevated CO_2 strengthened this correlation, indicating
405 enhanced benefits from nitrogen fixation (Figure 3E). Together, these results demonstrate that our
406 nodule detection model is well suited for application in research settings, providing a high-

407 throughput, rapid and reliable alternative to the laborious manual counting while also serving as a

408 proxy indicator of a plant's BNF activity.

409

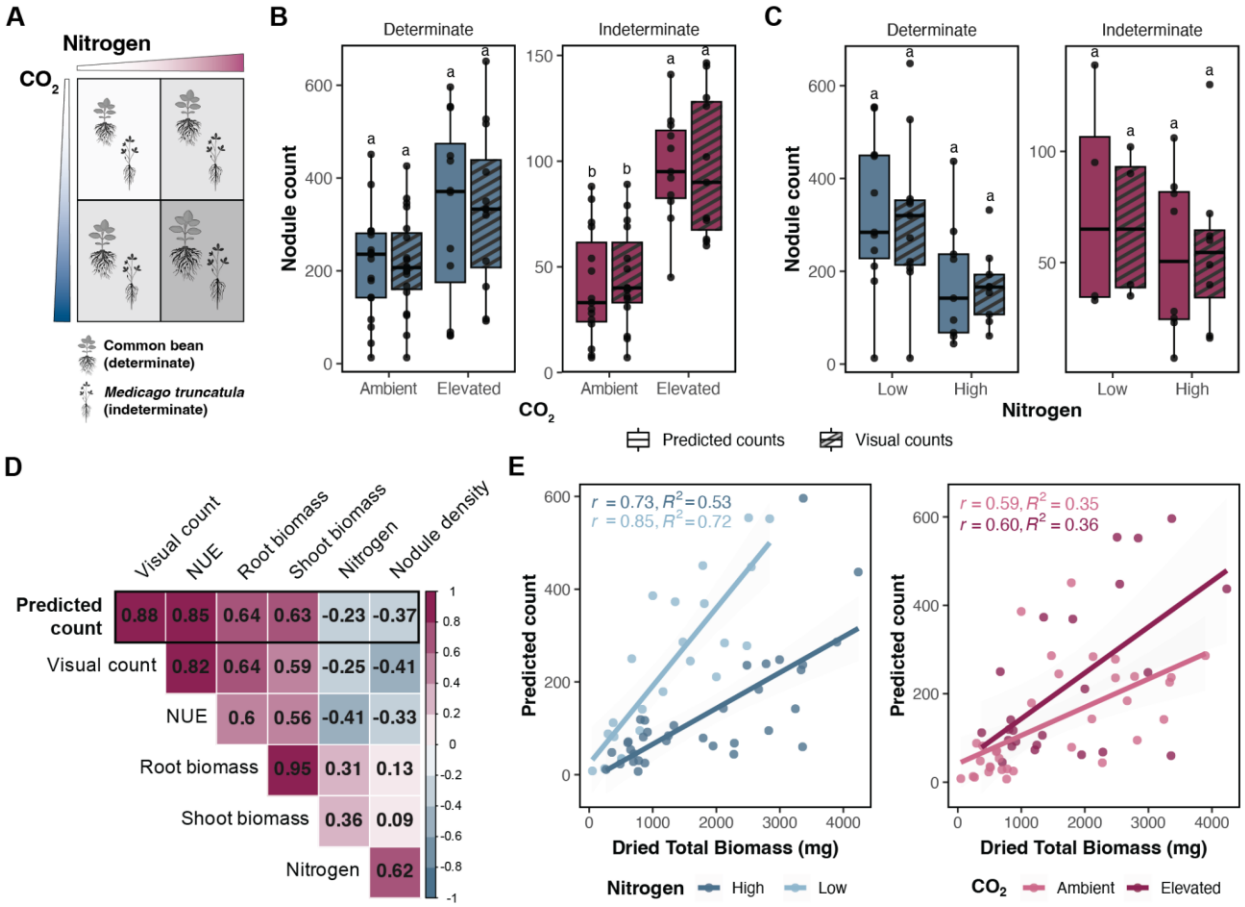

410

411 **Figure 3** Models trained on hyperspectral-enhanced images accurately capture variation in

412 nodulation patterns under different environmental conditions. (A) Experimental design showing

413 nitrogen and CO_2 treatments applied to bean and Medicago plants. (B) Quantification of nodules

414 under CO_2 treatments. (C) Quantification of nodules under nitrogen treatments (low = 5 mM NO_3^-

415 and high = 20 mM NO_3^-). (D) Correlation of predicted counts with physiological traits. (E)

416 Relationship between predicted nodule counts and total biomass across nitrogen and CO_2

treatments. Statistical significance in (B) and (C) was assessed using two-way ANOVA followed by Tukey's post hoc test.

Discussion

Understanding the symbiotic relationship is crucial for future crop improvement (Peoples et al., 1995). Nodule quantification is often used as a rapid reference for estimating BNF activity. However, acquiring such data typically relies on manual data collection by researchers, a process that is time-consuming, labor-intensive, and prone to human error. Here, we present an image-based nodule detection model as an alternative approach for efficient and standardized nodule quantification.

Spectral wavelength act as standard of nitrogen-fixing nodule detection

Given the importance of nodule quantification in assessing symbiotic performance, researchers have made multiple attempts to standardize the data collection process, with ongoing efforts aimed at improving its efficiency and scalability. Most approaches begin with image-based detection, leveraging nodules' visual features to identify and quantify nodules in a non-destructive manner. However, these approaches typically rely on semi-automated detection models trained solely on RGB images, with nodule identification still dependent on manual preprocessing by human annotators (Chung et al., 2020; Lira and Smith, 2000; Vikman and Vessey, 1993). Because nodules must be manually marked prior to model training or counting, these methods still require a consistent visual standard for defining what constitutes a nodule. To identify nodules, researchers often rely on visual cues such as physical irregularities or "bumpy" characteristics along the root axis (Chung et al., 2020), or look for circular structures in the images (Hensley et al., 2021).

However, such standards are inherently subjective and may limit consistency across different species, particularly when nodules vary in size, shape, and contrast against the root background, or when root orientation differs across images. Moreover, identification based purely on morphological characteristics does not capture the functional status of nodules, and therefore fails to quantify nodulation in terms of symbiotic efficiency (Remmler et al., 2014). To examine the level of nitrogen fixation, destructive chemical assays are required, typically involving nodule dissection, biochemical and isotopic analyses to quantify hemoglobin content (Wilson and Reisenauer, 1963), nitrogenase activity and nitrogen accumulation (Hardy et al., 1968; Vance et al., 1979). However, such methods remain time-consuming, low-throughput, and indirect, as they rely on measurements that do not capture dynamic changes in fixation activity.

In our approach, by utilizing three targeted spectral wavelengths (515 nm, 560 nm and 600 nm), we were able to clearly distinguish nodule tissue from root structures in the hyperspectral enhanced images. We demonstrate that the selected wavelengths are likely indicative of leghaemoglobin content, a key indicator of nitrogen fixation activity (Navascués et al., 2012). By using leghaemoglobin as an anchor for nodule identification, this approach provides a more standardized way of distinguishing nodules from root tissue and offers a more biologically relevant assessment of nitrogen fixation in a non-destructive manner. Furthermore, closer examination of the enhanced images revealed that nitrogen-fixing nodules exhibited varying levels of spectral enhancement, which may correspond to differences in nitrogen-fixing efficiency. Thus, this imaging approach not only accurately distinguishes nodules from root tissue but also holds a promising future for assessing nitrogen fixation activity and capturing developmental dynamics at the level of individual nodules.

Nodule detection pipeline allows time-efficient high-throughput nodule quantification

Past research has explored various approaches for nodule identification, including manual annotation of images and direct isolation of nodules for downstream counting analysis (Chang et al., 2024; Hensley et al., 2021; Woo et al., 2023). All of these methods require substantial time and labor for sample preprocessing. This often involves carefully spreading out the root systems to avoid overlapping structures and ensuring full exposure of all nodules, which can be particularly challenging under high nodule density or complex root architecture. In contrast, because our model captures nodule-specific spectral wavelengths that remained detectable even under partial root obstruction, the sample preprocessing is significantly simplified, requiring only that roots are reasonably spread out as long as a compatible soil mix is used.

Following the sample preprocessing, many previous studies have demonstrated successful nodule quantification; however, few have compared their program outputs to actual visual counts or evaluated their relationship with physiological traits. Two studies (Lira and Smith, 2000; Vikman and Vessey, 1993) that reported the accuracy of their image-based nodule detection models showed correlation coefficients (r) ranging from 0.85 to 0.89, which is comparable to our model's performance (r ranging from 0.89 to 0.96), with our model having a simpler sample preprocessing pipeline. Previous automated nodule counting efforts have largely focused on legumes with determinate nodules, with limited adaptation for indeterminate types likely due to their complex, branched morphology. Our morphotype-specific model enables accurate automated quantification of indeterminate nodules ($r \geq 0.90$), reporting the first successful implementation and offering scalability across diverse legume species.

While previous studies have explored the use of HSI to segment belowground structures such as roots and nodule-like features under varying conditions (Chang et al., 2024), few have

focused specifically on functional nodule identification or quantitative phenotyping using advanced object detection models. Our work demonstrates that integrating HSI with cutting-edge detection algorithms like YOLOv11 offers a scalable, high-throughput, and functionally informative approach to legume nodule phenotyping. The automated nodule counting program developed using YOLOv11 is user-friendly and computationally efficient, requiring only ~20 milliseconds per image on an NVIDIA A100 GPU (Figure S4). This rapid processing speed supports high-throughput phenotypic analysis with large datasets.

Model limitations and future directions

Several practices should be considered to ensure optimal detection performance. First, removing soil particles will improve nodule prediction accuracy, especially when using substrates like BM6 potting mix, which will obscure nodule visibility if densely covering the plant tissue, or turface, which shares a similar spectral wavelength as nitrogen-fixing nodules (Figure 1G). Residual fine white silica sand on nodules has minimal impact. Second, the timing of imaging post-harvest is important. Roots should be imaged after cleaning with minimal water; delays longer than 24 hours may lead to drying of nodules and degradation of leghaemoglobin content, which reduces image enhancement quality. Root tissue can be frozen and then thawed before imaging without a negative impact. Third, a high-resolution hyperspectral camera (with at least 900 pixel resolution) is needed for detailed detection of nodules on the images. For researchers without access to a hyperspectral imaging system, an alternative approach is to use narrow-band filters centered at 515 nm, 560 nm, and 600 nm to capture nodule-specific reflectance. By capturing individual images at each of these wavelengths and subsequently combining them, an enhanced

composite image can be generated that highlights nodules with improved contrast relative to root tissue.

Based on the comparison between predicted counts and visual counts, our nodule detection model effectively captures the overall trend in nodule number per image. However, variations in nodule size across different species can lead to deviations in the predicted count accuracy (Figure 2E). Tightly clustered nodules often lead to inaccurate counts, as their combined spectral signal can be overly intense, obscuring the boundaries between individual nodules and hiding the possible small nodules behind, resulting in a single, merged detection of a large nitrogen-fixing area. From the case study, the inhibition of nodulation in plants forming indeterminate nodules is less apparent (Figure 3C). Since indeterminate nodules maintain active meristematic tissue (Xiao et al., 2014), the growth and expansion of existing nodules may be favored over the initiation of new ones, leading to smaller observable changes in nodule count. With these limitations in mind, further development of the nodule quantification pipeline can help improve its accuracy and applicability. To address challenges of morphological differences among nodules across species, expanding the training dataset to include a wider range of root images with diverse nodule traits can further enhance the model's generalizability. An alternative strategy could involve quantifying the total nitrogen-fixing area rather than discrete nodule counts for tightly clustered nodules and quantifying physiological response on indeterminate nodules.

Acknowledgements

We thank Matthew Brooks for his foundational role in initiating and guiding this project and for his invaluable input throughout its course. Michelle McReynolds, Ely Lubash and Drew Kim for their assistance with experimental work and Seldon Kwafo for designing and constructing the rhizobox system. We also thank Ana Saballos, Jinwook Kim, Laurie Leonelli, and Katy Heath for providing seeds and rhizobial strains for experiments.

References

Appleby, C.A., 1984. Leghemoglobin and Rhizobium Respiration. Annu. Rev. Plant Physiol. 35, 443–478. https://doi.org/10.1146/annurev.pp.35.060184.002303

Barbedo, J.G.A., 2012. Method for Automatic Counting Root Nodules Using Digital Images, in: 2012 12th International Conference on Computational Science and Its Applications. Presented at the 2012 12th International Conference on Computational Science and Its Applications (ICCSA), IEEE, Salvador, Bahia, Brazil, pp. 159–161. https://doi.org/10.1109/ICCSA.2012.39

Behmann, J., Steinrücken, J., Plümer, L., 2014. Detection of early plant stress responses in hyperspectral images. ISPRS J. Photogramm. Remote Sens. 93, 98–111. https://doi.org/10.1016/j.isprsjprs.2014.03.016

Berdugo, C.A., Zito, R., Paulus, S., Mahlein, A. -K., 2014. Fusion of sensor data for the detection and differentiation of plant diseases in cucumber. Plant Pathol. 63, 1344–1356. https://doi.org/10.1111/ppa.12219

Bourion, V., Laguerre, G., Depret, G., Voisin, A.-S., Salon, C., Duc, G., 2007. Genetic Variability in Nodulation and Root Growth Affects Nitrogen Fixation and Accumulation in Pea. Ann. Bot. 100, 589–598. https://doi.org/10.1093/aob/mcm147

Chang, S.J., Chowdhry, R., Song, Y., Mejia, T., Hampton, A., Kucharski, S., Sazzad, T.M., Zhang, Y., Koppal, S.J., Wilson, C.H., Gerber, S., Tillman, B., Resende, M.F.R., Hammond, W.M., Zare, A., 2024. HyperPRI: A dataset of hyperspectral images for underground plant root study. Comput. Electron. Agric. 225, 109307. https://doi.org/10.1016/j.compag.2024.109307

Chung, Y.S., Lee, U., Heo, S., Silva, R.R., Na, C.-I., Kim, Y., 2020. Image-Based Machine

Learning Characterizes Root Nodule in Soybean Exposed to Silicon. Front. Plant Sci. 11. https://doi.org/10.3389/fpls.2020.520161

Dias, P.A.S., Melo, P.G.S., Pereira, H.S., Ferreira, E.P.D.B., 2017. Automated and estimation methods to count nodule number in common bean. Aust. J. Crop Sci. 11, 968–973. https://doi.org/10.21475/ajcs.17.11.08.pne452

Dupont, L., Alloing, G., Pierre, O., El, S., Hopkins, J., Hrouart, D., Frendo, P., 2012. The Legume Root Nodule: From Symbiotic Nitrogen Fixation to Senescence, in: Nagata, T. (Ed.), Senescence. InTech. https://doi.org/10.5772/34438

Fernández-Luqueño, F., Dendooven, L., Munive, A., Corlay-Chee, L., Serrano-Covarrubias, L.M., Espinosa-Victoria, D., 2008. Micro-morphology of common bean (Phaseolus vulgaris L.) nodules undergoing senescence. Acta Physiol. Plant. 30, 545–552. https://doi.org/10.1007/s11738-008-0153-7

Hardarson, G., Bliss, F.A., Cigales-Rivero, M.R., Henson, R.A., Kipe-Nolt, J.A., Longeri, L., Manrique, A., Pena-Cabriales, J.J., Pereira, P.A.A., Sanabria, C.A., Tsai, S.M., 1993. Genotypic variation in biological nitrogen fixation by common bean, in: Bliss, F.A., Hardarson, G. (Eds.), Enhancement of Biological Nitrogen Fixation of Common Bean in Latin America. Springer Netherlands, Dordrecht, pp. 59–70. https://doi.org/10.1007/978-94-011-2100-2_5

Hardy, R.W.F., Holsten, R.D., Jackson, E.K., Burns, R.C., 1968. The Acetylene-Ethylene Assay for N_2 Fixation: Laboratory and Field Evaluation. Plant Physiol. 43, 1185–1207. https://doi.org/10.1104/pp.43.8.1185

Hensley, D.A., Dukes, M.D., Zurweller, B.A., Rowland, D.L., 2021. Novel digital assessment technique used to describe peanut nodulation life history. Rhizosphere 19, 100374.

https://doi.org/10.1016/j.rhisph.2021.100374

Iqbal, N., Sadras, V.O., Denison, R.F., Zhou, Y., Denton, M.D., 2022. Clade-dependent effects of drought on nitrogen fixation and its components – Number, size, and activity of nodules in legumes. Field Crops Res. 284, 108586. https://doi.org/10.1016/j.fcr.2022.108586

Jocher, G., Qiu, J., 2024. Ultralytics YOLO11.

Libault, M., 2014. The carbon-nitrogen balance of the nodule and its regulation under elevated carbon dioxide concentration. BioMed Res. Int. 2014, 507946. https://doi.org/10.1155/2014/507946

Lira, M. de A., Smith, D.L., 2000. Use of a standard TWAIN scanner and software for nodule number determination on different legume species. Soil Biol. Biochem. 32, 1463–1467. https://doi.org/10.1016/S0038-0717(00)00052-3

Mergaert, P., Kereszt, A., Kondorosi, E., 2020. Gene Expression in Nitrogen-Fixing Symbiotic Nodule Cells in Medicago truncatula and Other Nodulating Plants. Plant Cell 32, 42–68. https://doi.org/10.1105/tpc.19.00494

Mortier, V., Holsters, M., Goormachtig, S., 2012. Never too many? How legumes control nodule numbers. Plant Cell Environ. 35, 245–258. https://doi.org/10.1111/j.1365-3040.2011.02406.x

Nagel, K.A., Putz, A., Gilmer, F., Heinz, K., Fischbach, A., Pfeifer, J., Faget, M., Blossfeld, S., Ernst, M., Dimaki, C., Kastenholz, B., Kleinert, A.-K., Galinski, A., Scharr, H., Fiorani, F., Schurr, U., 2012. GROWSCREEN-Rhizo is a novel phenotyping robot enabling simultaneous measurements of root and shoot growth for plants grown in soil-filled rhizotrons. Funct. Plant Biol. 39, 891. https://doi.org/10.1071/FP12023

Navascués, J., Pérez-Rontomé, C., Gay, M., Marcos, M., Yang, F., Walker, F.A., Desbois, A., Abián, J., Becana, M., 2012. Leghemoglobin green derivatives with nitrated hemes evidence production of highly reactive nitrogen species during aging of legume nodules. Proc. Natl. Acad. Sci. 109, 2660–2665. https://doi.org/10.1073/pnas.1116559109

Ott, T., van Dongen, J.T., Gu¨nther, C., Krusell, L., Desbrosses, G., Vigeolas, H., Bock, V., Czechowski, T., Geigenberger, P., Udvardi, M.K., 2005. Symbiotic Leghemoglobins Are Crucial for Nitrogen Fixation in Legume Root Nodules but Not for General Plant Growth and Development. Curr. Biol. 15, 531–535. https://doi.org/10.1016/j.cub.2005.01.042

Peoples, M.B., Herridge, D.F., Ladha, J.K., 1995. Biological nitrogen fixation: An efficient source of nitrogen for sustainable agricultural production? Plant Soil 174, 3–28. https://doi.org/10.1007/BF00032239

Redmon, J., Divvala, S., Girshick, R., Farhadi, A., 2015. You Only Look Once: Unified, Real-Time Object Detection. https://doi.org/10.48550/ARXIV.1506.02640

Remmler, L., Clairmont, L., Rolland-Lagan, A., Guinel, F.C., 2014. Standardized mapping of nodulation patterns in legume roots. New Phytol. 202, 1083–1094. https://doi.org/10.1111/nph.12712

Rogers, A., Ainsworth, E.A., Leakey, A.D.B., 2009. Will Elevated Carbon Dioxide Concentration Amplify the Benefits of Nitrogen Fixation in Legumes? Plant Physiol. 151, 1009–1016. https://doi.org/10.1104/pp.109.144113

Rowland, D.L., Smith, C., Cook, A., Mason, A., Schreffler, A., Bennett, J., 2015. Visualization of Peanut Nodules and Seasonal Nodulation Pattern in Different Tillage Systems Using a Minirhizotron System. Peanut Sci. 42, 1–10. https://doi.org/10.3146/0095-3679-42.1.1

Senthilkumar, M., Amaresan, N., Sankaranarayanan, A., 2021. Quantitative estimation of

leghemoglobin content in legume root nodules, in: Plant-Microbe Interactions. Humana, New York, NY, pp. 33–35. https://doi.org/10.1007/978-1-0716-1080-0_4

Skalski, P., 2019. Make Sense.

Sprent, J.I., 2007. Evolving ideas of legume evolution and diversity: a taxonomic perspective on the occurrence of nodulation. New Phytol. 174, 11–25. https://doi.org/10.1111/j.1469-8137.2007.02015.x

Sprent, J.I., Ardley, J., James, E.K., 2017. Biogeography of nodulated legumes and their nitrogen-fixing symbionts. New Phytol. 215, 40–56. https://doi.org/10.1111/nph.14474

Starker, C.G., Parra-Colmenares, A.L., Smith, L., Mitra, R.M., Long, S.R., 2006. Nitrogen Fixation Mutants of Medicago truncatula Fail to Support Plant and Bacterial Symbiotic Gene Expression. Plant Physiol. 140, 671–680. https://doi.org/10.1104/pp.105.072132

Tajima, R., Lee, O.N., Abe, J., Lux, A., Morita, S., 2007. Nitrogen-Fixing Activity of Root Nodules in Relation to Their Size in Peanut (*Arachis hypogaea* L.). Plant Prod. Sci. 10, 423–429. https://doi.org/10.1626/pps.10.423

TSYGANOV, V.E., VOROSHILOVA, V.A., PRIEFER, U.B., BORISOV, A.Y., TIKHONOVICH, I.A., 2002. Genetic Dissection of the Initiation of the Infection Process and Nodule Tissue Development in the Rhizobium–Pea (Pisum sativum L.) Symbiosis. Ann. Bot. 89, 357–366. https://doi.org/10.1093/aob/mcf051

van Noorden, G.E., Verbeek, R., Dinh, Q.D., Jin, J., Green, A., Ng, J.L.P., Mathesius, U., 2016. Molecular signals controlling the inhibition of nodulation by nitrate in medicago truncatula. Int. J. Mol. Sci. 17, 1060. https://doi.org/10.3390/ijms17071060

Vance, C.P., Heichel, G.H., Barnes, D.K., Bryan, J.W., Johnson, L.E., 1979. Nitrogen Fixation, Nodule Development, and Vegetative Regrowth of Alfalfa (*Medicago sativa* L.)

following Harvest. Plant Physiol. 64, 1–8. https://doi.org/10.1104/pp.64.1.1

Vikman, P.-$$$Ke, Vessey, J.K., 1993. Ontogenetic Changes in Root Nodule Subpopulations of Common Bean (*Phaseolus vulgaris* L.): III. NODULE FORMATION, GROWTH AND DEGRADATION. J. Exp. Bot. 44, 579–586. https://doi.org/10.1093/jxb/44.3.579

Wilson, D.O., Reisenauer, H.M., 1963. Determination of leghemoglobin in legume nodules. Anal. Biochem. 6, 27–30. https://doi.org/10.1016/0003-2697(63)90004-6

Woo, D., Ghimire, A., Jeong, S., Kim, Y., 2023. Soybean root image dataset and its deep learning application for nodule segmentation. Comput. Electron. Agric. 215, 108465. https://doi.org/10.1016/j.compag.2023.108465

Xiao, T.T., Schilderink, S., Moling, S., Deinum, E.E., Kondorosi, E., Franssen, H., Kulikova, O., Niebel, A., Bisseling, T., 2014. Fate map of medicago truncatula root nodules. Development 141, 3517–3528. https://doi.org/10.1242/dev.110775